CHAPTER

Conformation-based assay of tau protein aggregation

5

Yann Fichou, Neil A. Eschmann, Timothy J. Keller, Songi Han[1]

University of California Santa Barbara, Santa Barbara, CA, United States

[1]*Corresponding author: e-mail address: songi@chem.ucsb.edu*

CHAPTER OUTLINE

Abstract

Amyloid fiber-forming proteins are predominantly intrinsically disordered proteins (IDPs). The protein tau, present mostly in neurons, is no exception. There is a significant interest in the study of tau protein aggregation mechanisms, given the direct correlation between the deposit of β-sheet structured neurofibrillary tangles made of tau and pathology in several neurodegenerative diseases, including Alzheimer's disease. Among the core unresolved questions is the nature of the initial step triggering aggregation, with increasing attention placed on the question whether a conformational change of the IDPs plays a key role in the early stages of aggregation. Specifically, there is growing evidence that a shift in the conformation ensemble of tau is involved in its aggregation pathway, and might even dictate structural and pathological properties of mature fibers. Yet, because IDPs lack a well-defined 3D structure and

Methods in Cell Biology, Volume 141, ISSN 0091-679X, http://dx.doi.org/10.1016/bs.mcb.2017.06.008

continuously exchange between different conformers, it has been technically challenging to characterize their structural changes on-pathway to aggregation. Here, we make a case that double spin labeling of the β-sheet stacking region of tau combined with pulsed double electron–electron resonance spectroscopy is a powerful method to assay conformational changes occurring during the course of tau aggregation, by probing intramolecular distances around aggregation-prone domains. We specifically demonstrate the potential of this approach by presenting recent results on conformation rearrangement of the β-sheet stacking segment VQIINK (known as PHF6*) of tau. We highlight a canonical shift of the conformation ensemble, on-pathway and occurring at the earliest stage of aggregation, toward an opening of PHF6*. We expect this method to be applicable to other critical segments of tau and other IDPs.

1 INTRODUCTION

Proteins that do not have a well-defined 3D structure in their functional state are called intrinsically disordered proteins (IDPs). Their structural features can be described by ensembles of conformers that are likely to be adopted by the proteins. These ensembles are typically established by computer modeling combined with small angle scattering and/or NMR (Bernadó et al., 2005), and are collected in the protein ensemble database (PeDB) (Varadi et al., 2014). IDPs can often change from disordered to well-ordered states when interacting with binding partners (often referred to as folding upon binding; Wright & Dyson, 2009) or with themselves (i.e., aggregation) (Turoverov, Kuznetsova, & Uversky, 2010). Thus, IDPs can easily access lower energy minima reflecting (partially) folded states, which are reached by interacting with surrounding biomolecules (Turoverov et al., 2010). Their lack of well-defined structure challenges the dogmatic structure–function relationship and makes it more challenging to understand IDPs function and behavior.

The tau protein is an IDP that is found in neurons. By binding to tubulin molecules, tau modulates the growth and shrinkage of microtubules and is thus essential to the dynamics of the neuronal cytoskeleton (Feinstein & Wilson, 2005). Although this is the main known function, several other biological activities involving tau have been proposed, including regulation of axonal transport (Dixit, Ross, Goldman, & Holzbaur, 2008) and iron export (Lei et al., 2012) (see recent review by Wang & Mandelkow, 2016 for more details). Tau is primarily found inside neurons, however, evidence suggests that tau is also present and functional in the extracellular medium (Pooler, Phillips, Lau, Noble, & Hanger, 2013; Yamada et al., 2011, 2014). This extracellular tau might be involved in the progression of tau-associated diseases (Karch, Jeng, & Goate, 2012; Yamada et al., 2011).

The tau protein has attracted much attention because of its involvement in several neurodegenerative diseases, termed as tauopathies, which include Alzheimer's disease (AD) and frontotemporal dementia. The pathological relevance of tau was first discovered in AD where aggregates made of tau were found in patients' brains in the form of so-called paired-helical filaments (PHFs; see Goedert, Klug, & Crowther,

2006 for a good historical review). PHFs are composed of highly ordered fibers, called amyloid fibers, where the proteins are stacked in intermolecular β-sheets (Greenwald & Riek, 2010). Unraveling aggregation origin, pathways and pathogenicity is a topic of active research that has been gathered in several great reviews (see for instance, Chiti & Dobson, 2006; Greenwald & Riek, 2010; Ross & Poirier, 2005; Tipping, van Oosten-Hawle, Hewitt, & Radford, 2015; Wang & Mandelkow, 2016) and is not discussed here. It is worth noting that most studies use the cofactor heparin to model, in vitro, the pathological aggregation of tau (Goedert et al., 1996).

Emerging evidence shows that pathological tau can spread from neuron to neuron and trigger further aggregation by recruiting new monomers. Effectively, it means that tau fibers can "infect" surrounding healthy neurons and propagate through the brain (Clavaguera et al., 2009, 2014; de Calignon et al., 2012; Liu et al., 2012; Peeraer et al., 2015). Although what species actually spread from cell to cell is still unclear, it seems that small oligomers are the more likely candidates to traverse the cell membranes (Jackson et al., 2016; Lasagna-Reeves et al., 2012). Strikingly, tau fibers can adopt different arrangements, called strains, which sustain their characteristics over seeding, and lead to distinct tauopathies (Sanders et al., 2014). All together, these features have allowed the classification of tau as a prion-like protein (Goedert, 2015).

It is clearly established that the IDP tau undergoes a disorder-to-order transition, namely from a predominantly random-coil state to a β-sheets rich structure, during the course of aggregation into amyloid fibers. However, subtler intraprotein conformational variations are now pointed out as potential key features to understand aggregation mechanisms because (i) they may seed the aggregation pathway (Chirita, Congdon, Yin, & Kuret, 2005; Paudel & Li, 1999; Qi, Luo, Wei, Nussinov, & Ma, 2015), (ii) they may serve as a template in the prion mechanism (Falcon et al., 2015; Frost, Ollesch, Wille, & Diamond, 2009; Guo et al., 2016; Morozova, March, Robinson, & Colby, 2013), and (iii) they may template the different strains that dictate the fibers' pathological effect (Falcon et al., 2015; Sanders et al., 2014).

Despite the obvious interest and need in capturing conformational changes occurring during tau aggregation, there are hardly any direct experimental studies of such changes because few methods can assess them in solution state. NMR spectroscopy and small angle X-ray scattering are typically used to characterize structural features of IDPs (Bernadó et al., 2005), but cannot be easily applied to capture structural changes when aggregation occurs. Single-molecule FRET can measure intramolecular distances and has been used to measure large-domain tau conformational changes in the presence and absence of an aggregation inducer (Elbaum-Garfinkle & Rhoades, 2012). However, this study does not provide insight into the tau conformation evolution along aggregation time course. Ramachandran and coworkers have carried out UV resonance Raman spectroscopy to follow structural changes during aggregation (Ramachandran, Milán-Garcés, Udgaonkar, & Puranik, 2014); however, this method provided so far only a limited interpretation for the conformational changes that the protein undergoes. Most recently, Eschmann et al. presented an experimental proof that tau undergoes significant and distinct

conformational changes, in solution state, and on-pathway to amyloid fibers, in the earliest stages of aggregation well before β-sheet structures are formed (Eschmann et al., 2017). This study was based on the technique of pulsed electron paramagnetic resonance (EPR) dubbed double electron–electron resonance (DEER) or pulsed electron double resonance (PELDOR) (Milov, Ponomarev, & Tsvetkov, 1984; Pannier, Veit, Godt, Jeschke, & Spiess, 2000) applied to doubly spin-labeled tau (Eschmann et al., 2017).

DEER captures distances in the 1.5–8 nm range (Jeschke, 2012) between two electron spin labels that may be placed on the same protein or adjacent proteins in an assembly. A critical point is that DEER not only probes mean distances but also provides distance distributions, especially relevant for the IDPs. In addition, DEER can measure complex samples (e.g., mixtures of many molecules, large protein assemblies, or protein aggregates) as long as the EPR signal is unambiguously coming from the pair of spin labels. Because of these features, DEER has become a useful tool for obtaining structural information in biological systems (see for instance, review from Jeschke, 2012). Specifically, we present a method where DEER is used to measure intramolecular distances around β-sheet-forming segments of tau during the course of aggregation. These intra-tau distance measurements carried out on doubly spin-labeled tau complement previous EPR lineshape analysis studies that quantified inter-tau distances of single spin-labeled protein (Margittai & Langen, 2004) to unravel the β-sheet structure. The 1.5–8 nm distance range accessible by DEER is highly beneficial for this and other applications, especially as it allows to cover the cross section of many proteins, as well as average end-to-end distances of IDPs. The tradeoff for these advantages is that samples must be site specifically labeled at the distance measurement points. Access to the upper distance ranges of 7–8 nm requires special sample preparations, in particular in the case of aggregation-prone IDPs, and there continue to be advances in the developments of instrumentation, pulse shaping methods and sample preparations that push the maximum DEER-accessible distance to 8 nm and beyond (Borbat, Georgieva, & Freed, 2013; Schmidt, Wälti, Baber, Hustedt, & Clore, 2016; Spindler et al., 2015).

We present a method that combines site-specific double spin labeling and the pulsed dipolar EPR technique of DEER as a viable and generally applicable approach to track the conformations of tau and other IDPs during aggregation. The high biological impact of this method is based on the hypothesis that the measurement of conformation ensemble shifts of IDPs during aggregation represents a powerful assay to track aggregation pathway and mechanisms, as well as to unravel the nature of the aggregation seed. We describe the experimental procedure for sample preparation, measurements, and data analysis, and show exemplary data on the study of structural transformation of tau as presented in Eschmann et al. (2017). Specifically, we show key conformational changes occurring in the aggregation-prone region flanking the PHF6* segments at the earliest stage of tau protein aggregation, with the extended PHF6* conformation maintained throughout the maturation of tau aggregation.

2 METHODS

2.1 EXPERIMENTAL APPROACH

The overall goal is to identify conformational features that are activated when aggregation occurs. One of the strengths of this method is the ability to focus on early stages of aggregation as we aim at measuring conformational changes that would initiate the aggregation procedure. The strategy is thus to measure intramolecular distances at several time points after triggering aggregation. For this, we used DEER spectroscopy that can probe the distance distribution between two spin labels attached to a protein. In the example shown from Eschmann et al. (2017), we flanked with two spin labels the aggregation-prone regions PHF6 and PHF6* (Li & Lee, 2006; von Bergen et al., 2001), allowing us to measure distances across these critical segments, and thus to link aggregation propensity with conformational rearrangements. In the next sections, we first describe the procedure to produce doubly spin-labeled tau protein suitable for DEER experiments. Then, we provide details about DEER theory, measurements procedure, and data analysis, before presenting the results obtained on tau aggregation.

2.2 SAMPLE PREPARATION

We used a truncated version of the tau protein, referred to as Δtau187, in which the N-terminus region of the full-length htau40 has been removed. Δtau187 contains the four microtubule-binding repeat domains as well as the C-terminus domain, yielding a total molecular weight of 22 kDa including a poly-histidine tag.

2.2.1 Protein expression and purification

Tau protein expression and purification can be accomplished in many ways and differing examples can be found throughout the literature and in this volume (see for instance, Barghorn, Biernat, & Mandelkow, 2005; Gallat et al., 2012). Here, we briefly describe one possible protocol that is based on Eschmann et al. (2017). The coding sequence of Δtau187, inserted in the pET28a expression vector, was transformed and grown in BL21 (DE3) *Escherichia coli* cells. A 10-mL LB broth starter culture was grown overnight while shaking at 37°C and used to inoculate 1 L of fresh LB. Upon growing to an optical density of 0.6–0.8 at 600 nm, tau expression was induced by the addition of isopropyl β-D-thiogalactopyranoside to a final concentration of 1 mM before shaking at 37 °C for an additional 3 h. The *E. coli* cells were harvested by centrifuging the culture at $5000 \times g$ for 20 min.

Cell lysis was then carried out in 20–30 mL of lysis buffer (Tris–HCl, pH 7.4, 100 mM NaCl, 0.5 mM EDTA) with the addition of 1 protease inhibitor tablet (Thermo Scientific Pierce Protease inhibitor tablets, prod #88266) and 1 mM phenylmethane sulfonyl fluoride. Enzymatic lysis was started by the addition of lysozyme (40 mg per 1 L of culture) supplemented with DNase (20 μg/mL) and $MgCl_2$ (10 mM) for a total of 30 min on ice. Physical lysis was then carried out by three rounds of

freeze fracture in liquid nitrogen. Cell debris were removed by centrifugation at $13{,}000 \times g$ at 4°C for 10 min. The supernatant was then heated to ~65°C for 15 min to precipitate contaminating proteins. This processing step is possible due to tau's unique heat-resistant property. The solution was then cooled on ice for 20 min and centrifuged at $13{,}000 \times g$ at 4 °C for 10 min to pellet the precipitated proteins. The tau-supernatant was loaded onto a Ni-NTA agarose column and washed with 20 mL of buffer A (20 mM sodium phosphate, pH 7.0, 500 mM NaCl, 10 mM imidazole, and 100 μM EDTA), 12 mL of buffer B (20 mM sodium phosphate, pH 7.0, 1 M NaCl, 20 mM imidazole, 0.5 mM DTT, and 100 μM EDTA) and another 10 mL of buffer A. The protein was eluted by the addition of buffer C (20 mM sodium phosphate, pH 7.0, 0.5 mM DTT, and 100 mM NaCl) containing increasing amounts of imidazole; 1 mL of C1 (with 100 mM imidazole final), 6 mL of C2 (200 mM) and 10 mL of C3 (300 mM). The fractions were analyzed on a SDS-Page gel and the pure tau fractions collected and combined.

Several double-cysteine tau mutants were obtained by site-directed mutagenesis to probe distances at varying locations in the protein. All mutants were successfully purified using the above procedure for protein expression and purification.

2.2.2 Labeling strategy

The use of EPR for structural biology requires modification and spin-labeling of proteins, because they do not contain any unpaired electrons, unless bound to a metal center. The most popular method for introducing an unpaired electron spin tag into the system is to undergo site-directed spin labeling (SDSL) with the nitroxide label (1-oxyl-2,2,5,5,-tetramethylpyrroline-3-methyl)methanethiosulfonate (MTSL), which readily attaches to cysteine residues. Because all cysteines are labeled in this procedure, one might have to mutate away undesired natural cysteine residues before introducing new ones at the sites of interests. To achieve intraprotein distance measurements for the purpose of probing conformational features of tau, two sites on the same protein must be labeled. In the case of Δtau187, we mutated away the two natural cysteine (C291S and C322S), and we introduced new cysteines at the desired locations. Furthermore, it is essential to remain in dilute conditions, i.e., where the labeled proteins are far enough from each other to ensure that no interprotein distances are probed. This condition is easy to satisfy for solutions of soluble and stable proteins, but harder to meet for aggregating proteins as the spin labels from adjacent proteins within an aggregate may approach closely. In particular, amyloid fibers are highly compact and ordered aggregates, in which proteins form cross-β-sheet structures and intermolecular distances can be as close as ~5 Å. The approach we have taken is to "dilute" the spin labels by mixing MTSL-labeled tau with tau that is labeled with a diamagnetic probe. For the latter case, we used (1-acetoxy-2,2,5,5-tetramethyl-δ-3-pyrroline-3-methyl) methanethiosulfonate, which also attaches to cysteines, is chemically similar to MTSL, but has no unpaired electron (see Fig. 1). Typically, DEER measurements are sensitive to distances ranging from ~2–8 nm (Jeschke, 2012) although the exact distance range and sensitivity depends on the electron dephasing relaxing time T_M of the sample (see Section 2.3). For Δtau187 fibers,

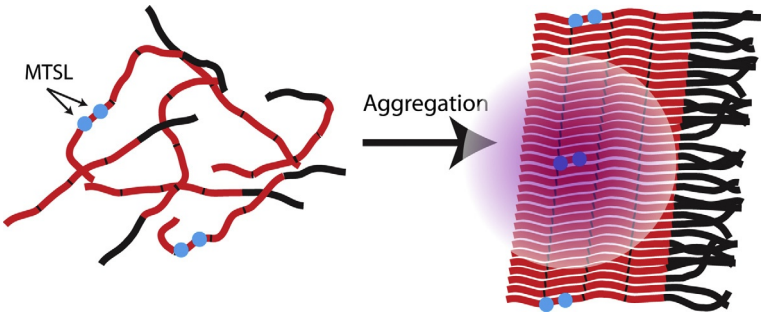

FIG. 1

The intrinsically disordered protein (IDP) tau (*left*) can undergo aggregation into neatly ordered β-sheet fibers (*right*). In order to prevent any unwanted interprotein spin interactions during DEER measurements, protein labeled with MTSL (*blue dots*) must be diluted with non-EPR-active protein.

we have shown that spin dilutions ranging from 1:15 down to 1:80 probe very similar distance distributions, suggesting that the lower dilution factor is adequate to avoid unwanted artifacts from inter-tau distances due to β-sheets stacking (Eschmann et al., 2017).

The specific method of SDSL adopted in our studies is as follows. Purified tau was treated with 5–10 mM DTT to ensure all cysteines were reduced. DTT was removed with a PD-10 desalting column and a 10× excess of the spin label compared to cysteines was added and allowed to react overnight at 4°C. Excess label was then removed with a PD-10 desalting column.

2.2.3 Inducing tau aggregation in vitro

The self-assembly of tau in vitro into PHF's does not occur spontaneously, even at relatively high protein concentrations, and typically requires the addition of cofactors to facilitate aggregation. One of the most popular methods used throughout the literature to induce fibrillation of tau is the addition of the polyanionic cofactor heparin (Goedert et al., 1996). This is a widely used method of initiating aggregation as well as the preferred method we have utilized to study the conformational changes of tau during the course of aggregation. Heparin is added at a 4:1 (Δtau187:heparin) molar ratio, which corresponds to a charge ratio of +54:−50 (Δtau187:heparin) at pH 7.0 (von Bergen, Barghorn, Biernat, Mandelkow, & Mandelkow, 2005). Specifically, the charge of Δtau187 at pH 7.0 is roughly +13.5, while the 11-kDa-heparin has an average charge of −50 making the total charge ratio +54:−50 for a 4:1 M ratio of Δtau187:heparin. Aggregation is often tracked via Thioflavin T (ThT), which fluoresces in the presence of amyloid patterns, while larger fibers can be directly imaged by transmission electron microscopy (see Fig. 2).

The addition of heparin is not the only method to induce aggregation of tau in vitro. There are several other cofactors which have been successfully used

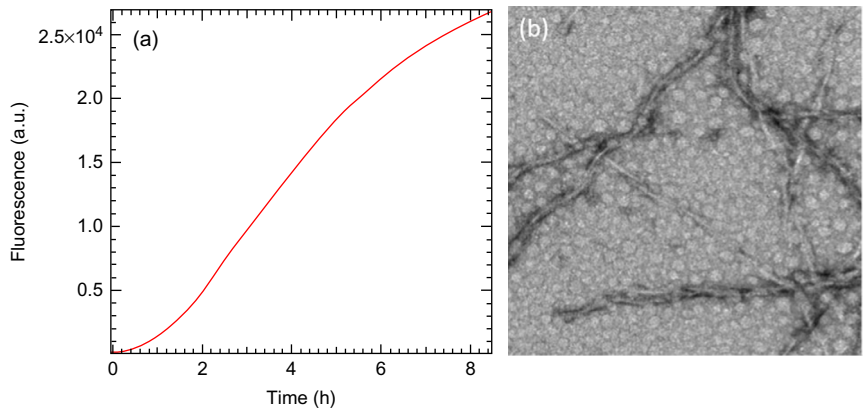

FIG. 2

(A) Thioflavin T fluorescence probes the formation of tau amyloid fibers. Heparin, which triggers tau aggregation, is added to tau solution at time 0. (B) Amyloid fibers can be imaged by negative-staining electron microscopy.

including arachidonic acid (Wilson & Binder, 1997), RNA (Kampers, Friedhoff, Biernat, Mandelkow, & Mandelkow, 1996), acidic peptides (Friedhoff, Schneider, Mandelkow, & Mandelkow, 1998), and carboxylated microspheres (Chirita et al., 2005). Another method is to induce filament formation through successive seeding from preformed fibers. This aggregation method is of particular interest because the use of brain-extracted seeds is thought to accurately replicate the type of fibers found in vivo (Morozova et al., 2013). The protocol described herein is applied for the tracking of early stages of heparin-induced aggregation of tau, but any other aggregation inducers could in principle be used.

2.3 DOUBLE ELECTRON–ELECTRON RESONANCE

DEER is a pulsed EPR method that allows for the measurement of distances in the 2–8 nm range between paramagnetic spin labels (Jeschke, 2012). We review here briefly the basic theory behind DEER before detailing the experimental procedure and data analysis method. The method is illustrated on the example of the aggregation of Δtau187 into amyloid fibers.

2.3.1 Theory

Let us briefly review the key equations behind a DEER experiment. We present the dipolar Hamiltonian for weakly coupled electron spins and demonstrate that the DEER signal comes from an average over all orientations. With the secular approximation, we can use the product operator formalism to calculate the time-domain signal modulated by the dipolar frequency, ω_{ee}, resulting from the DEER measurement. The rigorous analysis of the time-domain DEER signal allows to obtain a distance distribution from the DEER traces by Tikhonov regularization or an appropriate model fit.

The Hamiltonian for a pair of isolated spins $S_A = ½$ and $S_B = ½$ in the rotating frame is given by Schweiger and Jeschke (2001):

$$H = \Omega_A S_z^A + \Omega_B S_z^B + H_{dd} \tag{1}$$

In this equation, Ω_A (Ω_B) is the resonance offset for spin A (B), and S_z^A (S_z^B) is the spin operator for the z-component of the magnetization for spin A (B). H_{dd} is the Hamiltonian expressing the magnetic dipole–dipole interaction (Weil & Bolton, 2007)

$$H_{dd} = \frac{1}{r^3}\frac{\mu_0}{4\pi\hbar} g_A g_B \beta_e^2 \left[\boldsymbol{S}_A \boldsymbol{S}_B - \frac{3}{r^2}(\boldsymbol{S}_A \boldsymbol{r})(\boldsymbol{S}_B \boldsymbol{r}) \right] \tag{2}$$

where μ_0 is the magnetic permeability, $\hbar$ is Planck's constant divided by 2π, g_A, and g_B are the g-factors for spin A and B, β_e is the Bohr magneton, $\boldsymbol{S}_A$ and $\boldsymbol{S}_B$ represent the spin vector operators for electron spin A and B, r is a scalar value representing the distance between spin A and B, and $\boldsymbol{r}$ is a vector connecting spin A and B.

The Hamiltonian can be simplified if the difference in resonance offset for spin A and B is much greater than ω_{ee} ($|\Omega_A - \Omega_B| \gg \omega_{ee}$). In this case, we can ignore all nonsecular terms in the Hamiltonian (Eq. 2), and thus the Hamiltonian becomes diagonal as in Eq. (3).

$$H = \Omega_A S_z^A + \Omega_B S_z^B + \omega_{ee} S_z^A S_z^B \tag{3}$$

For interspin distances greater than 2 nm, any contribution from exchange coupling to the dipolar frequency, ω_{ee}, can be neglected and ω_{ee} is given by

$$\omega_{ee} = \frac{1}{r^3}\frac{\mu_0}{4\pi\hbar} g_1 g_2 \beta_e^2 \left(3\cos^2\theta - 1\right) = \omega_{ee}^0 \left(3\cos^2\theta - 1\right) \tag{4}$$

Since the Hamiltonian in Eq. (3) is already diagonal, the energy values can be obtained directly from the diagonal elements. The energy level diagram for this system is shown in Fig. 3A. The line for each spin is split into a doublet separated by ω_{ee} (Fig. 3B).

The angular dependence of the dipolar frequency gives rise to a Pake pattern in the spectral dimension when averaging over all possible orientations, θ (Fig. 4A–D). The frequency of the two maxima in the Pake pattern corresponds to ω_{ee}^0 in Eq. (4), and can be used to obtain an average distance for the given sample. Assuming a g-factor of 2.00, the distance between the two spins is

$$r\,(\mathrm{nm}) = \sqrt[3]{\frac{2\pi 52.04\,\mathrm{MHz}}{\omega_{ee}^0}} \tag{5}$$

Now that we have shown the Hamiltonian for a weakly coupled pair of spin ½, we can use the result to calculate the outcome of the 4-pulse DEER pulse sequence and develop an understanding of the experiment.

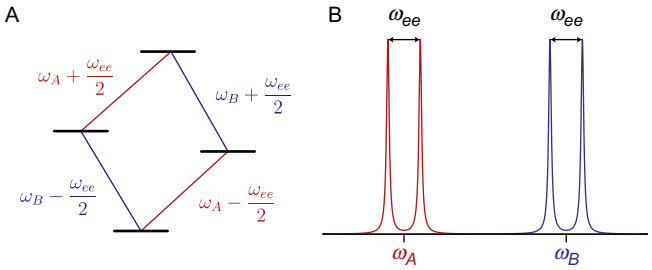

FIG. 3

(A) Energy level diagram for two weakly dipolar coupled spins ($S = 1/2$). Each line is split into two lines separated by ω_{ee}. (B) Typical spectrum of (A) showing each line split into a doublet.

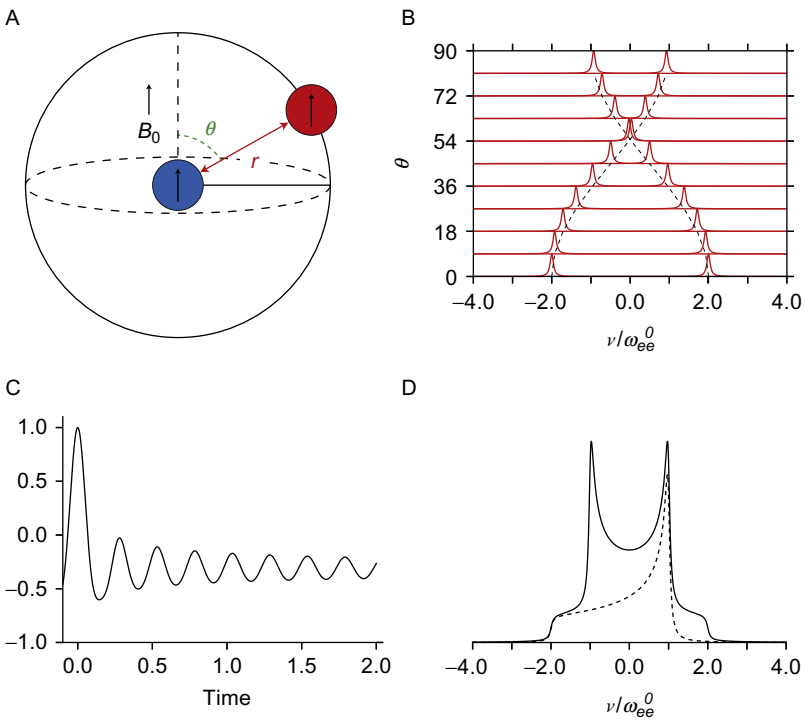

FIG. 4

(A) Definition of θ and r. (B) Angular dependence of ω_{ee}. (C) Time-domain DEER trace. and (D) Pake pattern (Fourier transform of time-domain DEER).

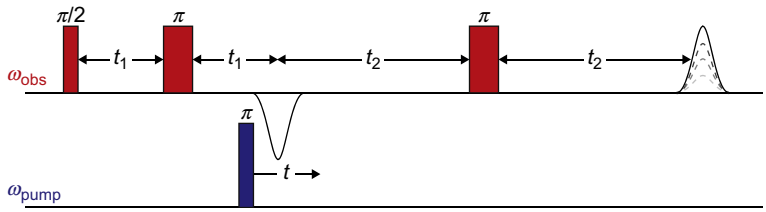

FIG. 5

Pulse sequence for 4-pulse DEER experiment. The position of the observe pulses (higher timeline) are held constant, while the position of the pump pulse is incremented (lower timeline).

2.3.2 Pulse sequence

The pulse sequence for 4-pulse DEER (Pannier et al., 2000) relies on a refocused Hahn echo sequence with an additional pump pulse (Fig. 5). In this experiment, the positions of the observe pulses are held constant and the position of the pump pulse stepped in time, while the integral of the refocused Hahn echo is measured. To understand the pulse sequence, we begin by assuming the observe and pump pulses are selective for spins A and B, respectively. At the position of the first Hahn echo ($\pi/2 - t_1 - \pi - t_1$), all magnetization is refocused; at time t the pump pulse will invert spin B and cause a shift in the resonance offset of spin A by $\Delta\Omega_A = \omega_{ee}t$. Depending on the time, spin A will now only refocus if $\omega_{ee}t = n(2\pi)$ ($n = 0, 1, 2\ldots$). The resulting signal $V_{AB}(t)$ is therefore a cosine function which is in fact the result given by application of the product operator formalism (Sørensen, Eich, Levitt, Bodenhausen, & Ernst, 1984) to the Hamiltonian in Eq. (3).

$$V_{AB}(t) = \cos(\omega_{ee}t) \tag{6}$$

The result from the product operator formalism (Eq. 6) is valid for a single orientation and ideal pulses. Several considerations are necessary in practice to model the signal for macroscopic samples (e.g., doubly labeled protein). Practical limitations on microwave power and spectral bandwidth ensure that complete excitation of B spins with the pump pulse does not occur. Thus, we rearrange Eq. (6), to include a modulation depth parameter, λ which will allow us to account for incomplete excitation of the B spins.

$$V_{AB}(t) = 1 - \lambda[1 - \cos(\omega_{ee}t)] \tag{7}$$

The modulation depth can take values between 0 and 1 and is equal to the fraction of B spins excited by the pump pulse (assuming 100% spin-labeling efficiency). As one can see from Eq. (7), this expression is equivalent to Eq. (6) in the case where $\lambda = 1$.

For experiments conducted on proteins, the sample is prepared in a frozen glass or powder. In this case, our macroscopic sample will contain an ensemble of dipolar coupled spins with the interspin vector, $\boldsymbol{r}$, oriented in every possible direction. Thus,

we take a powder average over a sphere to obtain the DEER signal (Schweiger & Jeschke, 2001):

$$V(t) = \int_0^{\pi/2} \sin(\theta) V_{AB}(t) \mathrm{d}\theta = 1 - \int_0^{\pi/2} \lambda(\theta) \sin(\theta) [1 - \cos(\omega_{ee}(\theta) t)] \mathrm{d}\theta \quad (8)$$

To express the DEER signal in a final form, we multiply $V(t)$ with a background function $B(t)$ to obtain $V_{\mathrm{DEER}}(t)$.

$$V_{\mathrm{DEER}}(t) = B(t) \left[1 - \int_0^{\pi/2} \lambda(\theta) \sin(\theta) [1 - \cos(\omega_{ee}(\theta) t)] \mathrm{d}\theta \right] \quad (9)$$

The given expression is valid for a single distance r and includes a background function $B(t)$ and the orientation dependent modulation depth $\lambda(\theta)$ (see later). The background function accounts for the fact that spin pairs do not exist in isolation, where interactions between spin pairs will also contribute to the DEER signal. For a homogenous distribution of spins, the sum of all dipolar couplings between spins gives rise to an exponential decay:

$$B(t) = \exp\left(-kCF_B t^{d/3}\right) \quad (10)$$

with

$$k = \frac{2\pi\mu_0 \beta_e^2 g_A g_B}{9\sqrt{3}\hbar} \quad (11)$$

where d is the dimensionality of the system ($d = 3$ for homogeneously distributed system in three dimensions), C is the spin concentration, and F_B is the fraction of B spins excited by the pump pulse.

The orientation-dependent modulation depth, $\lambda(\theta)$, must be considered in cases with excessive g- and hyperfine anisotropy, and where the molecular frames of spin A and B are highly correlated. Numerical simulations are required to treat orientation selection rigorously in biological samples. Fortunately, the flexibility of nitroxide spin labels makes orientation selection negligible for most cases with protein samples, except for DEER measurements at high frequencies of the order of 95 GHz (e.g., W-band) or higher.

2.3.3 Experimental considerations

With few exceptions (Meyer et al., 2015), DEER is performed at cryogenic temperatures. The optimal temperature is typically between 50 and 80 K for DEER with nitroxides (Fajer, Brown, & Song, 2007). At lower temperatures, the T_1 relaxation times become longer and the time between pulse sequences (shot-repetition time, SRT) must be increased to allow for thermal equilibrium to be recovered ($\mathrm{SRT}_{\mathrm{optimal}} = 1.2 \times T_1$). However, at higher temperatures, the electron phase memory

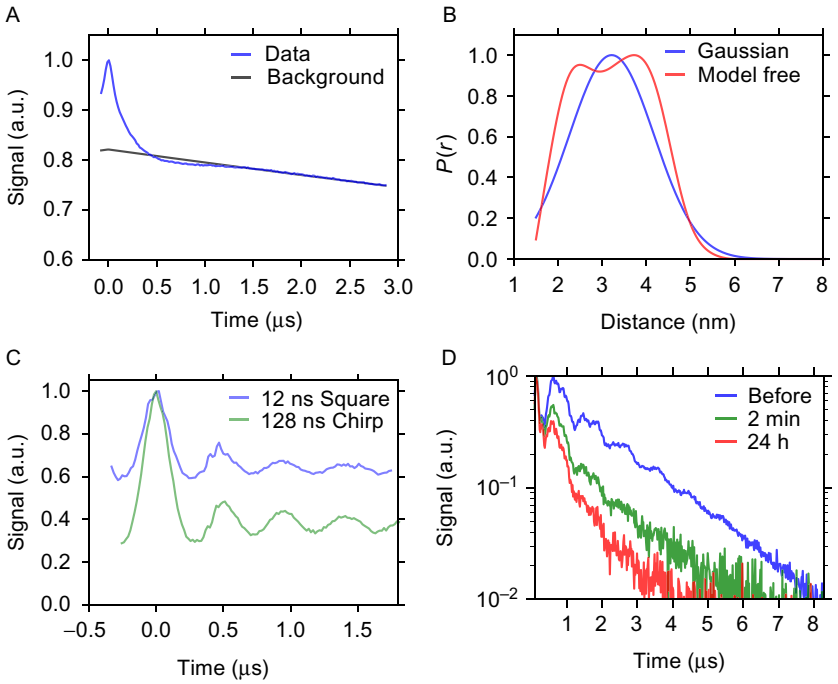

FIG. 6

(A) Q-band DEER data of Δtau187 labeled at G272C and S285C. (B) Distance distribution from Gaussian and model-free fit (obtained with LongDistances). (C) Shaped microwave pulses improve modulation depth by a factor of ~2. (D) Hahn echo decay for singly labeled Δtau187 S316C before heparin addition, 2 min after heparin addition, and 24 h after heparin addition. Pronounced oscillations in the decays are caused by deuterium and proton nuclear modulation (ESEEM; see the end of this section for more details).

time, T_M, becomes too short to fit sufficiently long dipolar evolution times to encode ω_{ee}^0.

Before the measurement, samples are typically vitrified in liquid nitrogen. To ensure glass formation upon freezing, ~30% (v/v) of cryoprotectant, such as glycerol or sucrose, is added (Georgieva et al., 2012). The cryoprotectant prevents the formation of ice crystals, which causes clustering of protein and leads to a decrease in T_M.

For aggregating samples, it is necessary to dilute the spin-labeled (Fig. 1; procedure detailed in Section 2.2.2) proteins with analogue (nonparamagnetic)-labeled proteins to prevent a dramatic decrease in the phase memory time T_M upon aggregation (Fig. 6D) as the spins closely approach each other when tau proteins stack in parallel to form β-sheet structured fibers. Spin dilution will also prevent interprotein distances from contributing to the distance distribution meant to capture intraprotein distances. For the tau protein, it was sufficient to use a 1:15 (spin labeled to analogue) dilution to diminish interferences from interprotein distances (see Section 2.2.2).

The signal-to-noise ratio (SNR) for a DEER measurement is an important issue that constrains the acceptable protein concentration in the sample as well as influences the measureable distance range. For longer distances, the required dipolar evolution time is greater because lower frequency oscillations cannot be recovered otherwise. If we neglect the lengths of the pulses, which are usually much shorter than delay periods t_1 and t_2, the maximum dipolar evolution time is equal to t_2 (Fig. 5). From the pulse sequence, we can see that the signal decays with T_M for a period of $2(t_1+t_2)$ before detection. Our SNR will therefore depend on the T_M of the sample and our choice of t_2. In addition, the SNR will not increase monotonically with concentration because higher concentrations of protein have shorter T_M due to instantaneous diffusion (Schweiger & Jeschke, 2001). In fact, the optimal protein concentration is related to the desired dipolar evolution time (Jeschke, 2012; Jeschke & Polyhach, 2007), but in many cases, it is >100 μM. In practice, the resources to synthesize or express the protein, the limited solubility or stability at high concentration of many proteins, as well as the interest in mimicking physiological concentrations justify method developments to enhance the sample sensitivity of DEER experiments and thus work at lower concentrations. The lower concentration limit, which varies from protein to protein, is about 50 μM of 100% spin-labeled Δtau187 measured on a DEER at X-band coupled with a 1 kW TWT amplifier. Due to a better SNR (Ghimire, McCarrick, Budil, & Lorigan, 2009; Polyhach et al., 2012), DEER at Q-band (35 GHz) coupled with a high-power amplifier (>30 W) can routinely measure protein concentrations as low as 10 μM. Typical sample volumes lie in the 10–40 μL range.

In order to extract reliable distance measurement from the DEER signal, it is necessary to average over multiple hours, often even days. Therefore, optimization of the experiment is paramount to improve SNR and reduce measurement times. In most cases, optimal SNR is achieved by pumping on the center of the nitroxide spectrum (Fig. 7B) as well as at the center of the resonator tuning dip, and by observing the EPR echo at +70 MHz off the edge of the tuning dip (Fig. 7A). This excitation scheme is chosen to maximize the modulation depth, to which the SNR is proportional. At X-band, when using a 12-ns pump pulse, a modulation depth of 0.3–0.5 is typically obtained. More recently, shaped microwave pulses have been used to increase the bandwidth of the pump pulse (Doll, Pribitzer, Tschaggelar, & Jeschke, 2013; Spindler, Glaser, Skinner, & Prisner, 2013). For nitroxides, an enhancement in modulation depth of ~2 has shown to be possible (Fig. 6C), leading to a dramatic increase in SNR by increasing the bandwidth of the pump pulse alone.

Electron spins are not isolated and exist in a lattice of nuclear spins which contribute to relaxation. A common method to limit this effect is to deuterate the protein and its environment, i.e., the solvent and/or the cryoprotectant. Deuterium nuclei do not contribute as strongly as protein to relaxation because their magnetic moment is less by a factor of ~7. By substituting protonated solvent with deuterated solvent, it is possible to extend T_M and thus increases the maximum dipolar evolution period resulting in an increase in the upper distance limit.

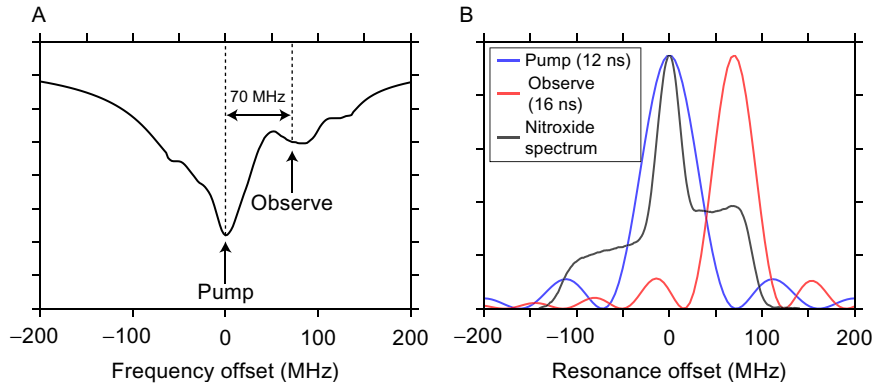

FIG. 7

X-band excitation scheme for DEER. (A) Experimental tuning dip of Bruker MS3-resonator. The resonator is maximally overcoupled to a *Q*-factor of 50–100 to maximize resonator bandwidth. The (B) field swept echo of a Δtau187 G272C/S285C before aggregation is shown in *black*, while typical pump and observe pulses are shown centered at resonance offsets of 0 and +70 MHz, respectively. Typical Q-band excitation scheme is similar such as to pump on the center of the tuning dip and maximum of the nitroxide spectrum.

Solvent deuteration is often a straightforward way to gain SNR, but further improvement can be achieved by additionally deuterating the protein. In the case of tau, solvent deuteration allows to increase possible distances from 3–4 to 5–6 nm. Protein and solvent deuteration is expected to extend this distance to about 7 nm.

A common artifact in DEER is caused by solvent nuclei which are weakly coupled to the electron spin. The only nuclei which are of concern for protein samples are solvent protons and deuteriums. Overlapping excitation profiles of the observed and pump pulses result in oscillations at frequencies which correspond to the Larmor frequency of nuclei coupled to the electron spin. This nuclear modulation effect is called electron spin echo envelope modulation (ESEEM) and is more prominent at X-band (9.5 GHz) than Q-band (35 GHz). Fortunately, since the phase of the ESEEM depends on t_1 (see Fig. 5 for t_1 definition), averaging multiple t_1 values can be used to remove ESEEM by destructive interferences. At X-band, the ESEEM effect from proton (14.5 MHz) and deuterium (2.2 MHz) can result in peaks emerging in the distance distribution centered around 1.53 and 2.9 nm, respectively. Proton ESEEM effects can be typically removed by averaging eight values of t_1 with increment of $\Delta t_1 = 8$ ns. Deuterium ESEEM can be similarly removed with eight of t_1 values spaced by $\Delta t_1 = 56$ ns. At Q-band, deuterium (8.2 MHz) gives a peak at 1.9 nm while the proton Larmor frequency (51 MHz) is too high for detection in the distance distribution of interest. Once we average over the t_1 dimension, we obtain the DEER signal as expressed in Eq. (9), and we can process the data to obtain a distance distribution.

2.3.4 Data analysis

Once we have obtained our DEER signal, $V_{DEER}(t)$ in Eq. (9), our next task is to convert this into a distance distribution, $P(r)$. The background signal is removed by fitting $V_{DEER}(t)$ to Eq. (10) and dividing by the background function to give the background corrected DEER signal $V(t)$ (Eq. 8). Finding the distance distribution from the time-domain DEER signal, $V(t)$, amounts to solving the following equation for the distance distribution, $P(r)$:

$$V(t) = \int_{R_{min}}^{R_{max}} \kappa(r,t)P(r)dr \tag{12}$$

where $\kappa(r,t)$ is referred to as the kernel function and represents the ensemble average over all dipolar couplings for a given r. This problem takes the form of the Fredholm equation and is an example of an inverse problem (Hansen, 1992a, 1992b). Solving this problem is approached by discretizing $\kappa(r,t)$ into a matrix and using an appropriate algorithm to find $P(r)$. Each column in the matrix $\kappa(r,t)$ is a DEER trace for a single distance corresponding to $P(r)$. In reality, any amount of noise in $V(t)$ are greatly amplified in the distance distribution $P(r)$, making our problem so-called ill-posed.

One method of solving ill-posed problems is Tikhonov regularization. This is a common method for obtaining distance distributions from DEER (Chiang, Borbat, & Freed, 2005a, 2005b). Tikhonov regularization assumes that the underlying distribution must be smooth. A regularization parameter determines the smoothness of the solution and therefore acts as a low pass filter. The optimal regularization parameter can be found by the L-curve method (Hansen, 1992a, 1992b).

Alternatively, a model-based fit can also be used, particularly in cases with broad distance distributions as well as limited SNR. The advantage of model-based fits is the ability to obtain error bars on fits. While it is possible to obtain error bars in Tikhonov regularization, detailed analysis has only been given recently (Edwards & Stoll, 2016) and error bars are often omitted from published data. Model fits on the other hand often will give meaningful error in both width and center of a distribution. With an IDP such as tau, the distance distributions are expected to be quite broad. It is often the case that a Gaussian distribution and Tikhonov regularization will fit equally well. If error estimates are of concern, the Gaussian fit will have the advantage of providing both distribution mean and width errors.

Several software packages are available to model DEER data, which include DeerAnalysis, LongDistances, and DEFit. LongDistances (Altenbach, n.d.) is a labview-based user-friendly package for processing data. It utilizes parallel processing and caching to increase performance and provides a highly visual environment for interacting with and processing data in real time. Another common program for processing DEER data is DeerAnalysis (Jeschke et al., 2006), which is written in MATLAB. Both of these programs include Tikhonov regularization as well as a number of model fits. They also conveniently indicate the ranges where the distance distributions and mean distances are reliable. Lastly, a software package which

allows fitting DEER data to multiple Gaussian distributions is called DeFit, which was written in MATLAB.

2.4 EXAMPLE DEER DATA OF TAU DURING AGGREGATION

In all, there are many aspects and conditions to consider when running DEER distance measurements, especially on IDPs. As an example, here we describe the experimental parameters and conditions chosen for intraprotein distance measurements of tau, which led to the discovery of an aggregation-prone conformation (Eschmann et al., 2017). While several mutants and constructs were used in Eschmann et al. (2017), here we focus on one construct, namely Δtau187 G272C/S285C. This mutant has cysteine residues introduced at positions G272 and S285, i.e., on each side of the aggregation-prone segment PHF6* (VQIINK). We used DEER at X- (∼10 GHz), as well as Ku-band (∼17 GHz) to measure the intramolecular distance between these two sites as a function of aggregation time. The concentration chosen for this sample was 50 μM of doubly spin-labeled tau protein that was then spin diluted by a factor of 15 with tau protein doubly labeled with the MTSL analogue label (750 μM analogue protein concentration). With these concentrations of tau, the total radical concentration is sufficiently high to obtain good signal-to-noise at Ku-band (but not at X-band), while the total tau concentration (800 μM) is kept within reason.

The cryoprotectant chosen for tau distance measurements was 30 wt% sucrose. Note that glycerol was not use due to the formation of protein precipitate in the presence of heparin, instead of the typical fiber formation pathway. Deuterated buffer and sucrose were used in order to maximize the T_M relaxation time. Samples were placed inside a 2.55 mm o.d. × 1.8 mm i.d. pyrex capillary and flash frozen in liquid nitrogen at the aggregation times of interests. Distance measurements were then conducted at 60 K using the 4-pulse DEER sequence (Fig. 5). T_M relaxation times were sufficiently long to measure DEER using t_2 times between 3 and 3.2 μs. The background was subtracted from the raw data using either a linear or second-order polynomial. The corrected time-domain traces (Fig. 8A–C) were then fitted using Tikhonov regularization to obtain the distance distribution information (Fig. 8D–F). Fig. 8D shows a significant change in distances already minutes after adding heparin, although the aggregation process is an hour timescale (Fig. 2A). After 12 h (Fig. 8F), the distance has increased from 3.16 to 4.35 nm, demonstrating a significant opening of the PHF6* domain during aggregation (Eschmann et al., 2017). Interestingly, similar results were found for another aggregation-prone region, PHF6 (VQIVYK), where a dramatic conformational change from compact to extended was shown. The fact that changes are observed at early times of aggregation suggests that tau first undergoes a misfolding step into an aggregation-prone conformation, before amyloid fiber formation is able to occur. New drug development strategies could aim at targeting these specific misfolded conformations to prevent the formation of amyloid aggregates.

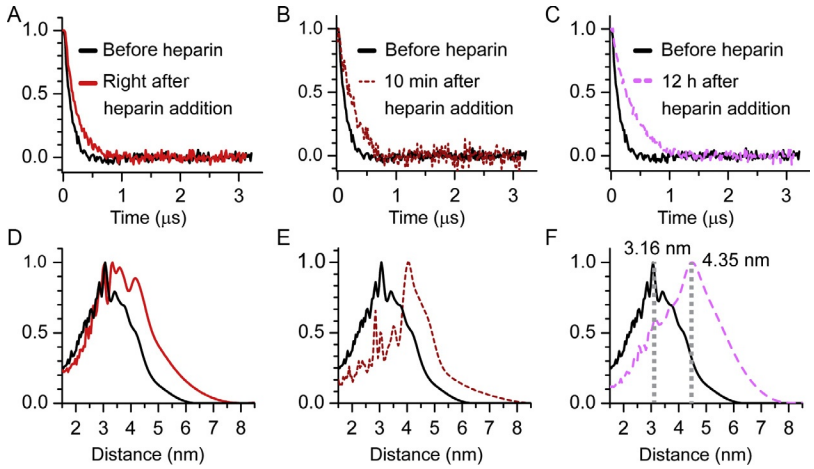

FIG. 8

Normalized DEER time-domain data taken at Ku-band (17.3 GHz) and corresponding distance distribution of Δtau187 G272C/S285C before heparin addition vs right after heparin addition (A and D, respectively), before heparin vs 10 min after heparin addition (B and E, respectively), and before heparin vs 12 h after heparin addition (C and F, respectively). All samples contain 50 μM MTSL-labeled tau and 750 μM analogue-labeled tau for a spin dilution of 1:15 to prevent any unwanted interspin artifacts. All samples also contain 30 wt% sucrose as a cryoprotectant.

Figure adapted from Eschmann, N., Georgieva, E., Ganguly, P., Borbat, P., Rappaport, M., Akdogan, Y., et al. (2017). Signature of an aggregation-prone conformation of tau. Scientific Reports, *7, 44739. https://doi.org/doi: 10.1038/srep44739.*

3 CONCLUSION

We have introduced a methodology to experimentally access protein misfolding and conformational changes happening during protein aggregation. By combining DEER spectroscopy and appropriate spin-labeling of strategically identified protein regions, one is able to measure protein intramolecular distance distribution and distance changes of the protein in solution upon vitrification. As DEER relies on unpaired-electron-containing spin probes that are not naturally present in proteins, it provides reliable distance measurements in both dilute conditions and local molecular crowding occurring in aggregation. Thus, DEER can provide a unique readout of the shifts of conformation ensemble occurring at any stage of protein aggregation.

One of the limitations of the method is the requirement of a high protein concentration. Because aggregation conditions force the use of spin dilution (see Section 2.2.2), the total protein concentration has to be about 10–15 times higher than the spin concentration required by the instrument. Although this point is improved by using a Q-band or Ku-band DEER that can measure spin concentrations as low as about 10 μM, i.e., protein concentration of 100–150 μM, it is still far above

in vivo protein physiological concentrations (typically in the nM to μM range). Because molar concentration (i.e., quantity of molecular unit per volume) is the parameter imposed by the instrument, this method is more suitable for low-molecular-weight proteins that can go to higher molar concentrations. The second main limitation of the presented technique is the detectable distance range. Although this range is ideally 2–8 nm, it depends in fact on the protein and was for tau about 2–5 nm. Thus, one has to pick the spin label sites carefully so that the distance between the labels remains in this range through the conformational changes. Without prior knowledge of the protein ensemble, it results in several trial-and-error steps to search for the suitable spin label locations. The main strategies to improve the detectable range are the use of deuterated buffers and proteins. Finally, spin labeling requires to mutate the protein, first to remove natively present cysteine residues, and second to introduce two new cysteine residues at the desired labeled locations. This process can destabilize the protein and/or modify its aggregation propensity. Comparing aggregation kinetics using ThT fluorescent assays is a typical way to monitor whether different mutants show similar aggregation properties.

The success of the method is demonstrated by the recent results obtained by Eschmann et al. showing conformational rearrangement occurring during tau aggregation (Eschmann et al., 2017). We measured the distance distribution across the aggregation-prone segment PHF6* to reveal whether its high aggregation propensity is correlated with a particular structural feature. We showed that a conformation shift toward an opening of PHF6* appears at a very early stage of aggregation and is on pathway to aggregation. Based on this experiment, we suggested that this conformational change is a direct observation of tau pathological, or misfolded, conformers that seed aggregation. Perspectives of the presented method include measurements of many distances within the protein to provide a complete picture of the pathological conformation ensemble. In addition, several aggregation conditions and triggers can be tested (for instance using different cofactors, such as RNA, or using pathological tau mutants, such as tau-P301L) to compare several aggregation pathways. For many or most amyloid forming IDPs, the core protein segments that stack into β-sheets are known, which provides an initial strategy for placing the two spin labels to probe local conformational changes. Thus, this method is expected to be applicable to other IDPs that share similar aggregation-induced pathological mechanisms, such as α-synuclein.

REFERENCES

Altenbach, C. (n.d.). https://sites.google.com/site/altenbach/labview-programs/epr-programs/long-distances.

Barghorn, S., Biernat, J., & Mandelkow, E. (2005). Purification of recombinant tau protein and preparation of Alzheimer-paired helical filaments in vitro. *Methods in Molecular Biology (Clifton, N.J.)*, *299*, 35–51.

Bernadó, P., Blanchard, L., Timmins, P., Marion, D., Ruigrok, R. W. H., & Blackledge, M. (2005). A structural model for unfolded proteins from residual dipolar couplings and small-angle X-ray scattering. *Proceedings of the National Academy of Sciences of the United States of America*, *102*(47), 17002–17007. http://dx.doi.org/10.1073/pnas.0506202102.

Borbat, P. P., Georgieva, E. R., & Freed, J. H. (2013). Improved sensitivity for long-distance measurements in biomolecules: Five-pulse double electron–electron resonance. *The Journal of Physical Chemistry Letters*, *4*(1), 170–175. http://dx.doi.org/10.1021/jz301788n.

Chiang, Y.-W., Borbat, P. P., & Freed, J. H. (2005a). Maximum entropy: A complement to Tikhonov regularization for determination of pair distance distributions by pulsed ESR. *Journal of Magnetic Resonance*, *177*(2), 184–196. http://dx.doi.org/10.1016/j.jmr.2005.07.021.

Chiang, Y.-W., Borbat, P. P., & Freed, J. H. (2005b). The determination of pair distance distributions by pulsed ESR using Tikhonov regularization. *Journal of Magnetic Resonance (San Diego, Calif.: 1997)*, *172*(2), 279–295. http://dx.doi.org/10.1016/j.jmr.2004.10.012.

Chirita, C. N., Congdon, E. E., Yin, H., & Kuret, J. (2005). Triggers of full-length tau aggregation: A role for partially folded intermediates. *Biochemistry*, *44*(15), 5862–5872. http://dx.doi.org/10.1021/bi0500123.

Chiti, F., & Dobson, C. M. (2006). Protein misfolding, functional amyloid, and human disease. *Annual Review of Biochemistry*, *75*(1), 333–366. http://dx.doi.org/10.1146/annurev.biochem.75.101304.123901.

Clavaguera, F., Bolmont, T., Crowther, R. A., Abramowski, D., Frank, S., Probst, A., et al. (2009). Transmission and spreading of tauopathy in transgenic mouse brain. *Nature Cell Biology*, *11*(7), 909–913. http://dx.doi.org/10.1038/ncb1901.

Clavaguera, F., Hench, J., Lavenir, I., Schweighauser, G., Frank, S., Goedert, M., et al. (2014). Peripheral administration of tau aggregates triggers intracerebral tauopathy in transgenic mice. *Acta Neuropathologica*, *127*(2), 299–301. http://dx.doi.org/10.1007/s00401-013-1231-5.

de Calignon, A., Polydoro, M., Suárez-Calvet, M., William, C., Adamowicz, D. H., Kopeikina, K. J., et al. (2012). Propagation of tau pathology in a model of early Alzheimer's disease. *Neuron*, *73*(4), 685–697. http://dx.doi.org/10.1016/j.neuron.2011.11.033.

Dixit, R., Ross, J. L., Goldman, Y. E., & Holzbaur, E. L. F. (2008). Differential regulation of dynein and kinesin motor proteins by tau. *Science*, *319*(5866), 1086–1089. http://dx.doi.org/10.1126/science.1152993.

Doll, A., Pribitzer, S., Tschaggelar, R., & Jeschke, G. (2013). Adiabatic and fast passage ultra-wideband inversion in pulsed EPR. *Journal of Magnetic Resonance*, *230*, 27–39. http://dx.doi.org/10.1016/j.jmr.2013.01.002.

Edwards, T. H., & Stoll, S. (2016). A Bayesian approach to quantifying uncertainty from experimental noise in DEER spectroscopy. *Journal of Magnetic Resonance*, *270*, 87–97. http://dx.doi.org/10.1016/j.jmr.2016.06.021.

Elbaum-Garfinkle, S., & Rhoades, E. (2012). Identification of an aggregation-prone structure of tau. *Journal of the American Chemical Society*, *134*(40), 16607–16613. http://dx.doi.org/10.1021/ja305206m.

Eschmann, N., Georgieva, E., Ganguly, P., Borbat, P., Rappaport, M., Akdogan, Y., et al. (2017). Signature of an aggregation-prone conformation of tau. *Scientific Reports*, *7*, 44739. http://dx.doi.org/10.1038/srep44739.

Fajer, P. G., Brown, L., & Song, L. (2007). Practical pulsed dipolar ESR (DEER). In *ESR spectroscopy in membrane biophysics* (pp. 95–128). US: Springer. Retrieved from http://link.springer.com/chapter/10.1007/978-0-387-49367-1_4.

Falcon, B., Cavallini, A., Angers, R., Glover, S., Murray, T. K., Barnham, L., et al. (2015). Conformation determines the seeding potencies of native and recombinant tau aggregates. *Journal of Biological Chemistry*, *290*(2), 1049–1065. http://dx.doi.org/10.1074/jbc.M114.589309.

Feinstein, S. C., & Wilson, L. (2005). Inability of tau to properly regulate neuronal microtubule dynamics: A loss-of-function mechanism by which tau might mediate neuronal cell death. *Biochimica et Biophysica Acta (BBA) - Molecular Basis of Disease*, *1739*(2–3), 268–279. http://dx.doi.org/10.1016/j.bbadis.2004.07.002.

Friedhoff, P., Schneider, A., Mandelkow, E. M., & Mandelkow, E. (1998). Rapid assembly of Alzheimer-like paired helical filaments from microtubule-associated protein tau monitored by fluorescence in solution. *Biochemistry*, *37*(28), 10223–10230. http://dx.doi.org/10.1021/bi980537d.

Frost, B., Ollesch, J., Wille, H., & Diamond, M. I. (2009). Conformational diversity of wild-type tau fibrils specified by templated conformation change. *Journal of Biological Chemistry*, *284*(6), 3546–3551. http://dx.doi.org/10.1074/jbc.M805627200.

Gallat, F.-X., Laganowsky, A., Wood, K., Gabel, F., van Eijck, L., Wuttke, J., et al. (2012). Dynamical coupling of intrinsically disordered proteins and their hydration water: Comparison with folded soluble and membrane proteins. *Biophysical Journal*, *103*(1), 129–136. http://dx.doi.org/10.1016/j.bpj.2012.05.027.

Georgieva, E. R., Roy, A. S., Grigoryants, V. M., Borbat, P. P., Earle, K. A., Scholes, C. P., et al. (2012). Effect of freezing conditions on distances and their distributions derived from double electron electron resonance (DEER): A study of doubly-spin-labeled T4 lysozyme. *Journal of Magnetic Resonance*, *216*, 69–77. http://dx.doi.org/10.1016/j.jmr.2012.01.004.

Ghimire, H., McCarrick, R. M., Budil, D. E., & Lorigan, G. A. (2009). Significantly improved sensitivity of Q-band PELDOR/DEER experiments relative to X-band is observed in measuring the inter-coil distance of a leucine zipper motif peptide (GCN4-LZ). *Biochemistry*, *48*(25), 5782–5784. http://dx.doi.org/10.1021/bi900781u.

Goedert, M. (2015). Alzheimer's and Parkinson's diseases: The prion concept in relation to assembled Aβ, tau, and α-synuclein. *Science*, *349*(6248), 1255555. http://dx.doi.org/10.1126/science.1255555.

Goedert, M., Jakes, R., Spillantini, M. G., Hasegawa, M., Smith, M. J., & Crowther, R. A. (1996). Assembly of microtubule-associated protein tau into Alzheimer-like filaments induced by sulphated glycosaminoglycans. *Nature*, *383*(6600), 550–553. http://dx.doi.org/10.1038/383550a0.

Goedert, M., Klug, A., & Crowther, R. A. (2006). Tau protein, the paired helical filament and Alzheimer's disease. *Journal of Alzheimer's Disease: JAD*, *9*(0), 195–207.

Greenwald, J., & Riek, R. (2010). Biology of amyloid: Structure, function, and regulation. *Structure*, *18*(10), 1244–1260. http://dx.doi.org/10.1016/j.str.2010.08.009.

Guo, J. L., Narasimhan, S., Changolkar, L., He, Z., Stieber, A., Zhang, B., et al. (2016). Unique pathological tau conformers from Alzheimer's brains transmit tau pathology in nontransgenic mice. *The Journal of Experimental Medicine*, *213*(12), 2635–2654. http://dx.doi.org/10.1084/jem.20160833.

Hansen, P. (1992a). Analysis of discrete Ill-posed problems by means of the L-Curve. *SIAM Review*, *34*(4), 561–580. http://dx.doi.org/10.1137/1034115.

Hansen, P. C. (1992b). Numerical tools for analysis and solution of Fredholm integral equations of the first kind. *Inverse Problems*, *8*(6), 849. http://dx.doi.org/10.1088/0266-5611/8/6/005.

Jackson, S. J., Kerridge, C., Cooper, J., Cavallini, A., Falcon, B., Cella, C. V., et al. (2016). Short fibrils constitute the major species of seed-competent tau in the brains of mice transgenic for human P301S tau. *The Journal of Neuroscience*, *36*(3), 762–772. http://dx.doi.org/10.1523/JNEUROSCI.3542-15.2016.

Jeschke, G. (2012). DEER distance measurements on proteins. *Annual Review of Physical Chemistry*, *63*(1), 419–446. http://dx.doi.org/10.1146/annurev-physchem-032511-143716.

Jeschke, G., Chechik, V., Ionita, P., Godt, A., Zimmermann, H., Banham, J., et al. (2006). DeerAnalysis2006—A comprehensive software package for analyzing pulsed ELDOR data. *Applied Magnetic Resonance*, *30*(3–4), 473–498. http://dx.doi.org/10.1007/BF03166213.

Jeschke, G., & Polyhach, Y. (2007). Distance measurements on spin-labelled biomacromolecules by pulsed electron paramagnetic resonance. *9*(16), 1895–1910. http://dx.doi.org/10.1039/B614920K.

Kampers, T., Friedhoff, P., Biernat, J., Mandelkow, E. M., & Mandelkow, E. (1996). RNA stimulates aggregation of microtubule-associated protein tau into Alzheimer-like paired helical filaments. *FEBS Letters*, *399*(3), 344–349.

Karch, C. M., Jeng, A. T., & Goate, A. M. (2012). Extracellular tau levels are influenced by variability in tau that is associated with tauopathies. *Journal of Biological Chemistry*, *287*(51), 42751–42762. http://dx.doi.org/10.1074/jbc.M112.380642.

Lasagna-Reeves, C. A., Castillo-Carranza, D. L., Sengupta, U., Guerrero-Munoz, M. J., Kiritoshi, T., Neugebauer, V., et al. (2012). Alzheimer brain-derived tau oligomers propagate pathology from endogenous tau. *Scientific Reports*, *2*, 700. http://dx.doi.org/10.1038/srep00700.

Lei, P., Ayton, S., Finkelstein, D. I., Spoerri, L., Ciccotosto, G. D., Wright, D. K., et al. (2012). Tau deficiency induces parkinsonism with dementia by impairing APP-mediated iron export. *Nature Medicine*, *18*(2), 291–295. http://dx.doi.org/10.1038/nm.2613.

Li, W., & Lee, V. M.-Y. (2006). Characterization of two VQIXXK motifs for tau fibrillization in vitro. *Biochemistry*, *45*(51), 15692–15701. http://dx.doi.org/10.1021/bi061422+.

Liu, L., Drouet, V., Wu, J. W., Witter, M. P., Small, S. A., Clelland, C., et al. (2012). Trans-synaptic spread of tau pathology in vivo. *PloS One*, *7*(2), e31302. http://dx.doi.org/10.1371/journal.pone.0031302.

Margittai, M., & Langen, R. (2004). Template-assisted filament growth by parallel stacking of tau. *Proceedings of the National Academy of Sciences of the United States of America*, *101*(28), 10278–10283.

Meyer, V., Swanson, M. A., Clouston, L. J., Boratyński, P. J., Stein, R. A., Mchaourab, H. S., et al. (2015). Room-temperature distance measurements of immobilized spin-labeled protein by DEER/PELDOR. *Biophysical Journal*, *108*(5), 1213–1219. http://dx.doi.org/10.1016/j.bpj.2015.01.015.

Milov, A. D., Ponomarev, A. B., & Tsvetkov, Y. D. (1984). Electron-electron double resonance in electron spin echo: Model biradical systems and the sensitized photolysis of decalin. *Chemical Physics Letters*, *110*(1), 67–72. http://dx.doi.org/10.1016/0009-2614(84)80148-7.

Morozova, O. A., March, Z. M., Robinson, A. S., & Colby, D. W. (2013). Conformational features of tau fibrils from Alzheimer's disease brain are faithfully propagated by

unmodified recombinant protein. *Biochemistry*, *52*, 6960–6967. http://pubs.acs.org/doi/abs/10.1021/bi400866w.

Pannier, M., Veit, S., Godt, A., Jeschke, G., & Spiess, H. W. (2000). Dead-time free measurement of dipole–dipole interactions between electron spins. *Journal of Magnetic Resonance*, *142*(2), 331–340. http://dx.doi.org/10.1006/jmre.1999.1944.

Paudel, H. K., & Li, W. (1999). Heparin-induced conformational change in microtubule-associated protein Tau as detected by chemical cross-linking and phosphopeptide mapping. *The Journal of Biological Chemistry*, *274*(12), 8029–8038.

Peeraer, E., Bottelbergs, A., Van Kolen, K., Stancu, I.-C., Vasconcelos, B., Mahieu, M., et al. (2015). Intracerebral injection of preformed synthetic tau fibrils initiates widespread tauopathy and neuronal loss in the brains of tau transgenic mice. *Neurobiology of Disease*, *73*, 83–95. http://dx.doi.org/10.1016/j.nbd.2014.08.032.

Polyhach, Y., Bordignon, E., Tschaggelar, R., Gandra, S., Godt, A., & Jeschke, G. (2012). High sensitivity and versatility of the DEER experiment on nitroxide radical pairs at Q-band frequencies. *Physical Chemistry Chemical Physics: PCCP*, *14*(30), 10762–10773. http://dx.doi.org/10.1039/c2cp41520h.

Pooler, A. M., Phillips, E. C., Lau, D. H. W., Noble, W., & Hanger, D. P. (2013). Physiological release of endogenous tau is stimulated by neuronal activity. *EMBO Reports*, *14*(4), 389–394. http://dx.doi.org/10.1038/embor.2013.15.

Qi, R., Luo, Y., Wei, G., Nussinov, R., & Ma, B. (2015). Aβ "Stretching-and-Packing" cross-seeding mechanism can trigger tau protein aggregation. *The Journal of Physical Chemistry Letters*, *6*(16), 3276–3282. http://dx.doi.org/10.1021/acs.jpclett.5b01447.

Ramachandran, G., Milán-Garcés, E. A., Udgaonkar, J. B., & Puranik, M. (2014). Resonance raman spectroscopic measurements delineate the structural changes that occur during tau fibril formation. *Biochemistry*, *53*(41), 6550–6565. http://dx.doi.org/10.1021/bi500528x.

Ross, C. A., & Poirier, M. A. (2005). What is the role of protein aggregation in neurodegeneration? *Nature Reviews Molecular Cell Biology*, *6*(11), 891–898. http://dx.doi.org/10.1038/nrm1742.

Sanders, D. W., Kaufman, S. K., DeVos, S. L., Sharma, A. M., Mirbaha, H., Li, A., et al. (2014). Distinct tau prion strains propagate in cells and mice and define different tauopathies. *Neuron*, *82*(6), 1271–1288. http://dx.doi.org/10.1016/j.neuron.2014.04.047.

Schmidt, T., Wälti, M. A., Baber, J. L., Hustedt, E. J., & Clore, G. M. (2016). Long distance measurements up to 160 Å in the GroEL tetradecamer using Q-band DEER EPR spectroscopy. *Angewandte Chemie International Edition*, *55*(51), 15905–15909. http://dx.doi.org/10.1002/anie.201609617.

Schweiger, A., & Jeschke, G. (2001). *Principles of pulse electron paramagnetic resonance*. Oxford, New York: Oxford University Press.

Sørensen, O. W., Eich, G. W., Levitt, M. H., Bodenhausen, G., & Ernst, R. R. (1984). Product operator formalism for the description of NMR pulse experiments. *Progress in Nuclear Magnetic Resonance Spectroscopy*, *16*, 163–192. http://dx.doi.org/10.1016/0079-6565(84)80005-9.

Spindler, P. E., Glaser, S. J., Skinner, T. E., & Prisner, T. F. (2013). Broadband inversion PELDOR spectroscopy with partially adiabatic shaped pulses. *Angewandte Chemie International Edition*, *52*(12), 3425–3429. http://dx.doi.org/10.1002/anie.201207777.

Spindler, P. E., Waclawska, I., Endeward, B., Plackmeyer, J., Ziegler, C., & Prisner, T. F. (2015). Carr–Purcell pulsed electron double resonance with shaped inversion pulses.

The Journal of Physical Chemistry Letters, *6*(21), 4331–4335. http://dx.doi.org/10.1021/acs.jpclett.5b01933.

Tipping, K. W., van Oosten-Hawle, P., Hewitt, E. W., & Radford, S. E. (2015). Amyloid fibres: Inert end-stage aggregates or key players in disease? *Trends in Biochemical Sciences*, *40*(12), 719–727. http://dx.doi.org/10.1016/j.tibs.2015.10.002.

Turoverov, K. K., Kuznetsova, I. M., & Uversky, V. N. (2010). The protein kingdom extended: Ordered and intrinsically disordered proteins, their folding, supramolecular complex formation, and aggregation. *Progress in Biophysics and Molecular Biology*, *102*(2–3), 73–84. http://dx.doi.org/10.1016/j.pbiomolbio.2010.01.003.

Varadi, M., Kosol, S., Lebrun, P., Valentini, E., Blackledge, M., Dunker, A. K., et al. (2014). pE-DB: A database of structural ensembles of intrinsically disordered and of unfolded proteins. *Nucleic Acids Research*, *42*(D1), D326–D335. http://dx.doi.org/10.1093/nar/gkt960.

von Bergen, M., Barghorn, S., Biernat, J., Mandelkow, E.-M., & Mandelkow, E. (2005). Tau aggregation is driven by a transition from random coil to beta sheet structure. *Biochimica et Biophysica Acta (BBA) - Molecular Basis of Disease*, *1739*(2–3), 158–166. http://dx.doi.org/10.1016/j.bbadis.2004.09.010.

von Bergen, M., Barghorn, S., Li, L., Marx, A., Biernat, J., Mandelkow, E. M., et al. (2001). Mutations of tau protein in frontotemporal dementia promote aggregation of paired helical filaments by enhancing local beta-structure. *The Journal of Biological Chemistry*, *276*(51), 48165–48174. http://dx.doi.org/10.1074/jbc.M105196200.

Wang, Y., & Mandelkow, E. (2016). Tau in physiology and pathology. *Nature Reviews Neuroscience*, *17*(1), 22–35. http://dx.doi.org/10.1038/nrn.2015.1.

Weil, J. A., & Bolton, J. R. (2007). *Electron paramagnetic resonance: Elementary theory and practical applications*. Hoboken, NJ: John Wiley & Sons.

Wilson, D. M., & Binder, L. I. (1997). Free fatty acids stimulate the polymerization of tau and amyloid beta peptides. In vitro evidence for a common effector of pathogenesis in Alzheimer's disease. *The American Journal of Pathology*, *150*(6), 2181–2195.

Wright, P. E., & Dyson, H. J. (2009). Linking folding and binding. *Current Opinion in Structural Biology*, *19*(1), 31–38. http://dx.doi.org/10.1016/j.sbi.2008.12.003.

Yamada, K., Cirrito, J. R., Stewart, F. R., Jiang, H., Finn, M. B., Holmes, B. B., et al. (2011). In vivo microdialysis reveals age-dependent decrease of brain interstitial fluid tau levels in P301S human tau transgenic mice. *Journal of Neuroscience*, *31*(37), 13110–13117. http://dx.doi.org/10.1523/JNEUROSCI.2569-11.2011.

Yamada, K., Holth, J. K., Liao, F., Stewart, F. R., Mahan, T. E., Jiang, H., et al. (2014). Neuronal activity regulates extracellular tau in vivo. *Journal of Experimental Medicine*, *211*(3), 387–393. http://dx.doi.org/10.1084/jem.20131685.